THE JOURNAL OF PHYSICAL CHEMISTRY B
A JOURNAL OF THE AMERICAN CHEMICAL SOCIETY

pubs.acs.org/JPCB

Article

Role of Unimers to Polymersomes Transition in Pluronic Blends for Controlled and Designated Drug Conveyance

Divya Patel, Nitumani Tripathi, Payal Vaswani, Germán Pérez-Sánchez, Dhiraj Bhatia, Ketan Kuperkar,* João A. P. Coutinho, and Pratap Bahadur

Cite This: https://doi.org/10.1021/acs.jpcb.4c00561

Read Online

ABSTRACT: This study investigates the nanoscale self-assembly from mixtures of two symmetrical poly(ethylene oxide)-poly(propylene oxide)-pol(ethylene oxide) (PEO–PPO-PEO) block copolymers (BCPs) with different lengths of PEO blocks and similar PPO blocks. The blended BCPs (commercially known as Pluronic F88 and L81, with 80 and 10% PEO, respectively) exhibited rich phase behavior in an aqueous solution. The relative viscosity (η_{rel}) indicated significant variations in the flow behavior, ranging from fluidic to viscous, thereby suggesting a possible micellar growth or morphological transition. The tensiometric experiments provided insight into the intermolecular hydrophobic interactions at the liquid–air interface favoring the surface activity of mixed-system micellization. Dynamic light scattering (DLS) and small-angle neutron scattering (SANS) revealed the varied structural morphologies of these core–shell mixed micelles and polymersomes formed under different conditions. At a concentration of ≤5% w/v, Pluronic F88 exists as molecularly dissolved unimers or Gaussian chains. However, the addition of the very hydrophobic Pluronic L81, even at a much lower (<0.2%) concentration, induced micellization and promoted micellar growth/transition. These results were further substantiated through molecular dynamics (MD) simulations, employing a readily transferable coarse-grained (CG) molecular model grounded in the MARTINI force field with density and solvent-accessible surface area (SASA) profiles. These findings proved that F88 underwent micellar growth/transition in the presence of L81. Furthermore, the potential use of these Pluronic mixed micelles as nanocarriers for the anticancer drug quercetin (QCT) was explored. The spectral analysis provided insight into the enhanced solubility of QCT through the assessment of the standard free energy of solubilization ($\Delta G°$), drug-loading efficiency (DL%), encapsulation efficiency (EE%), and partition coefficient (P). A detailed optimization of the drug release kinetics was presented by employing various kinetic models. The [3-(4,5-dimethylthiazol-2-yl)-2,5-diphenyltetrazolium bromide] MTT assay, a frequently used technique for assessing cytotoxicity in anticancer research, was used to gauge the effectiveness of these QCT-loaded mixed nanoaggregates.

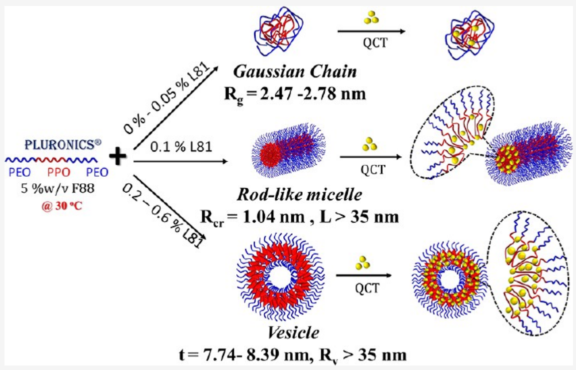

■ INTRODUCTION

Pluronics or poloxamers are commercially available poly(ethylene oxide)-poly(propylene oxide)-poly(ethylene oxide) (PEO–PPO-PEO) triblock copolymers (BCPs) that have attracted attention as polymeric surface-active noncytotoxic amphiphilic compound agents.[1−7] These BCPs offer a wide range of constitutional features with varying sizes of PEO and PPO blocks, total molecular weights, and diverse hydrophilic–lipophilic balance (HLB) values. These BCPs are often used in the solubilization of hydrophobic substances and delivery of poorly soluble drugs, in detergency, wetting, foaming, emulsification, lubrication, cosmetics, etc.[4,5,8−13] Over the past three decades, extensive research has been conducted on Pluronics due to their promising potential in these significant domains.[10−,,−17]

The temperature-dependent PEO and PPO units in Pluronics enable the formation of micelles at the critical micelle concentration (CMC) or critical micelle temperature (CMT). This is attributed to the hydrophobicity of the PPO chains that constitute the micelle core, while PEO chains form the hydrated shell of the micelle.[15−20] Additionally, these BCPs have been widely recognized as having reversible and thermorheological behavior in aqueous solutions.[7,9,20−23] Using the PPO and PEO compositions, the hydrophilicity of Pluronics

Received: January 26, 2024
Revised: May 17, 2024
Accepted: May 20, 2024
Published: June 7, 2024

Scheme 1. Details of the Chemicals Used in the Investigation[a]

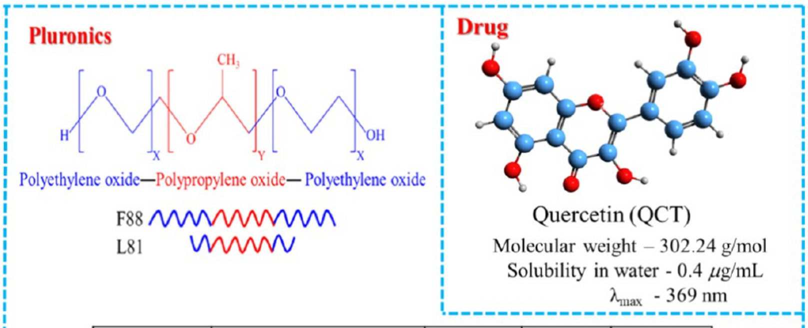

System	Nominal composition $EO_xPO_yEO_x$		Mol.wt. (Da)	HLB range	[a]CP (°C)
	X	Y			
F88	103	39	11400	>24	>100
L81	3	43	2750	1-7	20

[a]Cloud point (CP) values were taken from the reported literature for solutions of 5% w/v Pluronic concentration in water.[27,36,43]

can be easily fine-tuned, making them very versatile precursors with high drug-loading capacity in pharmaceutical applications.[24,25] Furthermore, mixed systems of Pluronics entail diverse amphiphilic characteristics and offer notable benefits, including favored micellization, micellar growth/transition (higher geometry such as rod-like micelles and vesicles),[26] improved kinetic stability of micelles, feasible drug-loading capacities, precise control over micelle size to prevent precipitation, and other factors that can enhance the efficiency of drug delivery systems.

Researchers have explored mixed Pluronic systems to develop more precise medical formulations.[7,22,27−35] For instance, Oh et al. investigated the stability of a mixed system of L121 and F127 and found the most stable combination that yields enhanced solubilization of hydrophobic dyes. Subsequently, numerous studies have been focused on the application of binary Pluronic systems, considering copolymers with similar PPO and varying PEO.[37] Kulthe et al. investigated L81/P123 mixtures that exhibit small particles and high solubilization potential.[38] Another study incorporated paclitaxel (PTX) drugs into a binary system of Pluronic L101 and P105 for the treatment of multidrug-resistant diseases.[40] By combining hydrophilic (F68, F87, F127, P85, P105) and hydrophobic (L61, L81, L101, L121) Pluronic, mixed micelles have been prepared and characterized.[38] Patel et al. examined the self-assembly and phase behavior of the P123 + F127 system with an enhanced quercetin (QCT) solubilization.[36] This study showed the modulations of the phase behavior and particle size profile of a Pluronic mixed micelle. Patel et al. observed that binary copolymeric solutions undergo progressive micellar growth on heating to cloud point temperature.[39]

Molecular dynamics (MD) simulations have become increasingly popular for studying surfactant self-assemblies. This allows researchers to study the formation of micelles, phase transitions, and the impact of different thermodynamic conditions on the self-assembly of amphiphilic compounds. MD simulations can provide valuable insights into nanoscale scenarios, beyond most experimental techniques. Bhendale et al. found an open- to folded-chain structural change upon increasing the concentration of Pluronic L64 through coarse-grained (CG) simulations. They found an increase in the aggregation number at lower concentrations and a micellar phase-to-lamellar phase transition when the concentration was raised.[40] Albano et al. employed MD simulations to investigate the characteristics of Pluronic F127 within micellar and lamellar phases.[41] Nie et al. revealed that Pluronic micelles can attain drug-loading capacities of 80%. Micelle shrinkage due to drug encapsulation is caused by the localized packing of hydrophobic−hydrophilic units. Water molecules were forced out of micelles in the presence of the drug. Previous coarse-grain (CG) computational and molecular dynamic (MD) simulations revealed the intricate scenario of the drug-releasing processes from polymeric micelles and they were in good agreement with the experimental results.[42]

Our study aims to create stable systems by mixing hydrophilic F88 (5 wt %/v) with varying concentrations of hydrophobic L81. Although F88 did not form micelles at low concentrations, the addition of L81 promoted micellization and growth and induced a shape transition in the examined systems. Detailed physicochemical characterization was performed to evaluate the intricate phase behavior and solution viscosity as a function of temperature. Further, dynamic light scattering (DLS) and small-angle neutron scattering (SANS) techniques were employed to elucidate the induced micellization with potential micellar growth/morphological transition from the evaluated parameters, such as the radius of gyration (R_g), cross-sectional radius of rod-like micelles (R_{cr}), length of rod-like micelles (L), and vesicle thickness (t). In addition, CG-MD simulations provided rational insight into the experimental results throughout the simulation trajectories, where micelle density profiles and solvent-accessible surface (SASA) areas are discussed. Finally, experimental and simulation results are accounted for to enhance solubilization and transport of the hydrophobic anticancer drug quercetin (QCT) by F88/L81 mixed micelles.

■ MATERIALS AND METHODS

Materials. BCPs (F88 and L81) were generously provided as gifts (BASF, Mumbai, India). The structural details are presented in Scheme 1. The anticancer drug quercetin (QCT) was purchased from Sigma-Aldrich (BRL, IN). No additional purification procedures were performed for these compounds prior to use. For neutron scattering tests, deuterium oxide (D_2O) with a D purity of 99.9% was used as a solvent to create a distinct contrast between the hydrophobic micellar core and the solvent. In other studies, double-distilled water was used to prepare the solutions. Before each measurement, the sample solutions were filtered using a nylon filter with a pore diameter of approximately 0.22 μm. All necessary glassware for the experiments was cleaned using chromic acid and rinsed with double-distilled water.

Methodology. *Phase Behavior, Surface Tension, and Solution Relative Viscosity.* The clouding behavior, expressed as the cloud point (CP), was measured by gradually heating the solution in a thin glass vial placed in a stirring heating bath. The concentration of F88 (5% w/v) was maintained, while the concentration of L81 was varied. CP corresponds to the temperature at which the solution exhibits a sudden turbid appearance above a certain temperature. For the sake of accuracy, CP measurements were performed at least three times, displaying a deviation within a range of ±0.2 °C.[15,18,25,33]

The surface activity of 5% w/v F88 in the absence and presence of L81 with increasing concentration were determined using a tensiometer (Model-K9, KRÜSS GMbH, Germany). Surface tension (γ) readings were sustained following the dilution method and recorded accurately within ±0.1 mN m^{-1} after temperature equilibration at 30 °C (within ±0.1 °C).[18,39]

The relative solution viscosity (η_{rel}) of each system was measured by subjecting the samples to temperature aging. A calibrated Cannon Ubbelohde viscometer was used to obtain η_{rel}, and all measurements were performed in a water bath with temperature fluctuations maintained within ±0.2 °C. The flow rate of the solutions was determined using a calibrated stopwatch, and the procedure was repeated at least three times with a deviation of ±5 s.[7,15,43]

Scattering Conduct. The hydrodynamic diameter (D_h) was determined using a dynamic light scattering (DLS) Zetasizer Nano device (Malvern Instruments, U.K.). The incident beam had a scattering angle of 90° and was generated using a 4 mW He−Ne laser at a wavelength of ∼635 nm. In this study, the sizes of the particles were specifically measured in numbers from the frequency distribution. Five consecutive measurements were considered for each sample to obtain the average particle size.[31,33,34,36] Additionally, to further investigate micellar size distributions and morphology transitions, small-angle neutron scattering (SANS) experiments were carried out at the Guide Tube Laboratory (Dhruva Reactor, BARC, India). The samples were prepared in D_2O and the coherent differential scattering cross-section ($d\Sigma/d\Omega$) per unit volume was evaluated as a function of wave vector transfer $Q = (4\pi \sin\theta/2)/\lambda$, where λ is the wavelength of the incident neutrons and θ is the scattering angle (SANS data was fitted with SASFIT software, as described in the Supporting Information section). The mean wavelength of the monochromatized beam was ∼5.26 Å with $\Delta\lambda/\lambda \sim 15\%$. The angular distribution of the scattered neutrons was recorded using a 1 m-long one-dimensional He^3 position-sensitive detector aligned horizontally. The instrument covered a Q-range of ∼0.017 to 0.35 Å^{-1}.[7,36,43−46]

Here, using the sphere model for spherical micelles, the ellipsoidal−core−shell model for ellipsoidal micelles, and the spherical shell-iii model for polymersomes (multilamellar vesicles), the differential scattering cross-section per unit volume ($d\Sigma/d\Omega$) was measured for a system of monodisperse particles in a medium:[47,48]

$$\left(\frac{d\Sigma}{d\Omega}\right)(Q) = nV^2(\rho_p - \rho_s)^2 P(Q)S(Q) + B \tag{1}$$

where n denotes the number density of particles, ρ_p and ρ_s are, respectively, the scattering length densities of the particle and solvent, and V is the volume of the particle. $P(Q)$ is the intraparticle structure factor and $S(Q)$ is the interparticle structure factor. In our case, $S(Q)$ is assumed to be unity, indicating that no interparticle correlations or interactions affect the scattering pattern. B is a constant term representing the incoherent background, which is mainly due to the hydrogen present in the sample.

The intraparticle structure factor $P(Q)$ is decided by the shape and size of the particle and is the square of the single-particle form factor $F(Q)$, as determined by

$$P(Q) = \langle |F(Q)|^2 \rangle \tag{2}$$

The form factor of Gaussian chain coils with the radius of gyration R_g is given by

$$P(Q) = 2\frac{\exp(-Q^2R_g^2) + Q^2R_g^2 - 1}{(Q^2R_g^2)^2} \tag{3}$$

The form factor of Gaussian chains is usually used to model the polymer molecules.[49] $P(Q)$ for Gaussian chains shows a slope of (−2) at higher Q values.

For a spherical particle of radius R, $F(Q)$ is given by[50]

$$F(Q) = 3\left[\frac{\sin(QR) - QR\cos(QR)}{(QR)^3}\right] \tag{4}$$

For a rod-like micelle of length $L = 2l$ and a cross-sectional radius R,[51]

$$P(Q) = \int_0^{\pi/2} \frac{\sin^2(Ql\cos\beta)}{Q^2l^2\cos^2\beta} \frac{4J_1^2(QR\sin\beta)}{Q^2R^2\sin^2\beta} \sin\beta \, d\beta \tag{5}$$

where β is the angle between the axis of the rod and bisectrix. J_1 is the Bessel function of order unity.

For a system of monodisperse unilamellar vesicles, $d\Sigma/d\Omega$ can be expressed as[51]

$$\frac{d\Sigma}{d\Omega}(Q, R) = n(\rho_v - \rho_s)^2 \left[\frac{4}{3}\pi R^3 \frac{3J_1(QR)}{QR} - \frac{4}{3}\pi(R+t)^3 \frac{3J_1[Q(R+t)]}{Q(R+t)}\right]^2 \tag{6}$$

where n is the number density of the vesicles, ρ_v and ρ_s are the scattering length densities of the vesicle bilayer and solvent, respectively, R is the radius of the vesicle, and t is the thickness of the bilayer. $J_1(x)$ is the first-order Bessel function and is given by

$$J_1(x) = \frac{\sin x - x\cos x}{x^2} \tag{7}$$

The polydispersity in the size distribution of particles is incorporated using the following integration[52]

https://doi.org/10.1021/acs.jpcb.4c00561
J. Phys. Chem. B XXXX, XXX, XXX−XXX

$$\frac{d\Sigma}{d\Omega}(Q) = \int \frac{d\Sigma}{d\Omega}(Q, R) f(R) dR + B \quad (8)$$

where $f(R)$ is the size distribution of the vesicles and is usually accounted for by a log-normal distribution as given by

$$f(R) = \frac{1}{\sqrt{2\pi} R\sigma} \exp\left[-\frac{1}{2\sigma^2}\left(\ln \frac{R}{R_{med}} \right)^2 \right] \quad (9)$$

where R_{med} is the median value and σ is the standard deviation (polydispersity) of the distribution. The mean radius (R_m) is given by $R_m = R_{med} \exp(\sigma^2/2)$.

The data were analyzed by comparing the scattering from the different models with the experimental data. Throughout the data analysis, corrections were made for instrumental smearing, where the calculated scattering profiles were smeared by the appropriate resolution function for comparison with the measured data.[25,53] The fitted parameters in the analysis were optimized using a nonlinear least-squares fitting program for model scattering.

Transmission Electron Microscopy (TEM). A JEOL JEM-1210 electron microscope with an accelerating voltage of 80 kV was used to obtain transmission electron microscopy (TEM) observations. One drop of the examined solution was applied to a copper grid on a glass plate to create the sample, which was then left to air-dry for a full day.[1,31]

Coarse-Grain Molecular Dynamics Simulations and Model Validation. CG-MD computer simulations were used to overcome the time- and size-scale limitations of all-atom simulations to investigate the self-assembly and phase behavior, especially when addressing relatively large molecules. Basically, CG-MD models group atoms with similar physicochemical characteristics in one interaction center, so-called beads, thereby decreasing the computational demand. The CG-MD simulations developed in this work were performed with the GROMACS 2023 package integrating Newton's equation of motion throughout the leapfrog algorithm with a 20 fs time step. The bonded energy contributions for the total potential energy entailed bond stretching and angle bending, constrained by the LINear Constraint Solver (LINCS). Nonbonded interactions were calculated with the Verlet cutoff scheme (potential-shift-Verlet modifiers) with a 1.2 nm cutoff and included the Lennard-Jones (LJ) potential and Coulomb interactions. Long-range electrostatic interactions were assessed with the particle-mesh-Ewald (PME). The temperature was fixed at 298.15 K with a coupling time constant of 2.0 ps, whereas the pressure was isotropically coupled at 1 bar with a time constant of 24.0 ps. The temperature and pressure were set using a velocity-rescaling thermostat and Parrinello−Rahman barostat, respectively. Simulation boxes, with periodic boundary conditions, were considered in all directions and built with Packmol.[54−61]

Prior to the NpT ensemble production runs, an energy minimization step was carried out with the steepest descent algorithm to avoid close contact between molecules. Afterward, two short NVT and NpT ensemble simulations were performed to determine the appropriate temperature and density, respectively. The total potential energy and simulated box densities were monitored to ensure equilibrium. The visual molecular dynamics (VMD) software package[62] was used to visualize the MD trajectories, whereas micellar size distributions were analyzed using an in-house code based on the Hoshen−Kopelman cluster counting algorithm.[63,64]

The CG-MD mapping of the molecules investigated in this work is summarized in Scheme 2. The model for F68 and L81

Scheme 2. CG Mapping of the F88 and L81 BCPs[a]

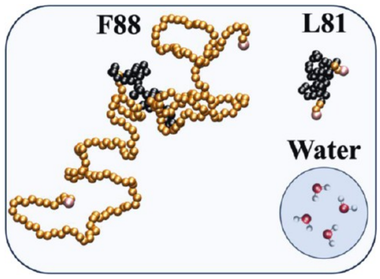

[a]Black and orange beads represent the PPO and PEO groups, respectively, whereas the terminal hydroxyl [CH_2−O−H] groups are colored pink. The CG-MD water model implicitly includes four atomistic water molecules.

was taken from Arash et al.,[65] whose parameterization follows that of Grunewald et al.[66] for PEO groups, whereas new PPO temperature-dependent parameters were developed and validated. In this model, important characteristics were accurately replicated, including the CMT and the presence of unimer phases below the CMT, in a variety of normal BCP systems with different molecular weights and PEO/PPO ratios. Additionally, the Arash et al. model includes an analysis of BCP micelle size distributions, which are in good agreement with the experimental results. The diffusion coefficients over a wide range of temperatures were also obtained.

In our work, simulation trajectories with a simulation time of 8000 ns were used to evaluate the self-assembly of F88 and L81, micelle growth, and phase transition. Postprocessing tools such as density profiles and SASA were used to provide a quantitative perspective. The micelle density profiles were obtained with a cluster counting code to provide insight into the three-dimensional spatial distribution of PEO and PPO groups in addition to water molecules. These profiles are crucial for understanding the structure of micelles and their interactions with the surrounding environment, allowing the investigation of how temperature, concentration, and BCP composition (including PPO and PEO lengths and ratios) impact the structure of micelles. In contrast, SASA can be used to determine the degree of hydration/dehydration of selected groups of molecules during the simulation. For instance, BCP micelles with a larger SASA of the micelle corona (PEO groups) are more exposed to water but should decrease when the temperature is raised, leading to a dehydration process.

Spectral Investigation. The anticancer drug quercetin (QCT) was added in excess to the Pluronic solutions to create drug-loaded solutions. To calculate the concentration of dissolved QCT, the absorbance was measured using a HachDR6000 spectrophotometer between 200 and 800 nm.[7,33,36,67] The sample solutions were filtered using a nylon syringe filter for each measurement (0.22 μm) to remove dust particles, if any. By employing well-known mathematical models, such as zero-order kinetics, first-order kinetics, and Higuchi, Hixson−Crowell, and Korsymeyer−Peppas models, the mechanism of QCT release from the blended micellar (5% w/v F88 as a function of L81 concentration) system was examined. Later, ethanol was added to the QCT-loaded Pluronic micelles to assess the drug-loading efficiency and

https://doi.org/10.1021/acs.jpcb.4c00561
J. Phys. Chem. B XXXX, XXX, XXX−XXX

drug-loading activity.[36,38,39] In addition, drug loading (DL), encapsulation efficiency (EE), partition coefficient (P), and standard free energy of solubilization ($\Delta G°$) were evaluated to ascertain the amount of QCT that could be solubilized into each micelle.[69] The drug loading and encapsulation efficiency were calculated usingthe equations:

$$\mathrm{DL} = \frac{m_{\mathrm{drug,micelle}}}{m_{\mathrm{drug+polymer,prep}}} \times 100\% \tag{10}$$

$$\mathrm{EE} = \frac{m_{\mathrm{drug,micelle}}}{m_{\mathrm{drug,prep}}} \times 100\% \tag{11}$$

where $m_{\mathrm{drug,micelle}}$ is the mass of drug in the micelle, $m_{\mathrm{drug+polymer,prep}}$ is the mass of drug plus polymer used in micelle preparation, and $m_{\mathrm{drug,prep}}$ is the mass of drug used in micelle preparation.

The partition coefficient is defined as the distribution of drugs between the micellar and aqueous phases:

$$P = \frac{D_{\mathrm{M}} - D_{\mathrm{W}}}{D_{\mathrm{W}}} \tag{12}$$

where D_{M} and D_{W} are the concentrations of the drug in the micelles and water, respectively.[38,39]

The standard free energy of solubilization (ΔG), i.e., the energy required to partition the QCT from the aqueous phase to the micellar phase, is calculated as follows:[42]

$$\Delta G = -RT \ln P \tag{13}$$

where R is the gas law constant and T is the absolute temperature.

Release Kinetics. In release kinetics, experiments for 5% w/v F88 with increased [L81] concentration were conducted in the presence of QCT utilizing the dialysis method.[43,44] A 2 mL solution with and without QCT-loaded F88 or its respective mixed micellar solution was maintained at a temperature of 30 ± 0.2 °C with continuous stirring at 150 rpm. At regular intervals, 2 mL samples of the examined solution were withdrawn. The samples were then filtered using an appropriate syringe filter before being subjected to QCT release estimation via spectrophotometric analysis. By following this experimental procedure, the release kinetics of QCT from the micellar formulations could be accurately investigated, providing valuable insights into their behavior under physiological conditions, which was further investigated using well-known mathematical models.

Zero-Order Model. Systems whose release rates are unrelated to the concentration of the soluble drug are described by the zero-order model. The following equation represents this mathematical concept:

$$Q_t = K_0 t \tag{14}$$

where Q_t is the total amount of QCT released as a function of time, K_0 is the zero-order rate constant, and t is the time of the release process.

First-Order Model. Systems whose release rates vary depending on the drug concentration are described by the first-order model:

$$\log C_t = -\frac{K_1 t}{2.303} \tag{15}$$

where t represents time, K_1 is the first-order rate constant, and C_t is the total amount of QCT remaining at time t.

Higuchi Model. It states that the square root of time denotes how quickly the drug leaves the body. Here, the drug release mechanism in this instance is based on Fick's law as follows:

$$Q_t = K_{\mathrm{H}} t^{1/2} \tag{16}$$

where Q_t is the total amount of QCT released at time t, K_{H} is the zero-order rate constant, and t is the passage of time.

Korsmeyer–Peppas Model. The power law model, which is straightforward and comprehensive, depicts how a drug is released from polymeric systems. The Korsmeyer–Peppas model is particularly helpful for explaining systems, where the release mechanism is intricate or multiple processes are involved, following the equation

$$Q_t = K_{\mathrm{kp}} t^n \tag{17}$$

where Q_t is the cumulative amount of QCT released at time t, and K_{kp} is the rate constant of Korsmeyer–Peppas, and n is the release exponent.[68,69]

Cell Culture. HeLa cells (Cervical cancer) were cultured and maintained in Dulbecco's modified Eagle's medium (DMEM, Gibco), supplemented with 10%v/v fetal bovine serum (FBS, Gibco) and 1%v/v Penstrep solution (Himedia, India) in a humidified incubator at 37 °C and 5% CO_2.[68]

In Vitro Cytotoxicity Assay. The cytotoxicity of all of the compounds was assessed using the MTT assay (3-(4,5-dimethylthiazol-2-yl)-2,5-diphenyl tetrasodium bromide, TCI) against the HeLa cell line. Cells were trypsinized, seeded into a 96-well plate for the assay, and allowed to adhere for 24 h. At 85–90% confluency, the cells were incubated for 4 and 12 h with a concentration gradient of the compounds. The medium was then decanted, and the cells were treated with 100 μL of MTT (5 mg/mL stock) prepared in 1× PBS and incubated at 37 °C for 4 h. The formed formazan crystals were solubilized in 100 μL of DMSO, and the absorbance was measured at 570 nm using a Multiplate reader (Biotech). The percentage viability was calculated by normalizing the absorbance value of the test sample with that of the untreated control. The curve was plotted for concentration vs normalized cell viability.[43,69]

Cellular Uptake of Compounds. HeLa cells were trypsinized and seeded in 12 well plates on coverslips. After attaining 80–90% confluency, the cells were treated with all compounds at different concentrations and incubated for 1 h at 37 °C. The medium was decanted, followed by a gentle PBS wash (2 times) of the cells. The cells were further fixed in a 4% paraformaldehyde (PFA) solution at 37 °C for 15 min. The cells were washed with PBS (3 times) to remove any residual PFA. The coverslips were then mounted on slides using Mowiol and Hoechst 33342 to stain the nucleus. The images were taken using a Leica Confocal Microscope at 512 × 512 format using a 405 nm laser. The images were further processed using Fiji ImageJ software.[68]

■ RESULTS AND DISCUSSION

Solution Behavior. F88 is a hydrophilic BCP with 80% EO content, yielding mostly unimers in aqueous solution, thereby exhibiting a CP > 100 °C.[46] Conversely, L81 is quite hydrophobic, with only 10% EO content forming vesicular structures displaying a relatively low CP > 20 °C.[7,33] Our experiments show that the CP of 5 wt %/v F88 decreases as a function of L81 concentration (Figure 1a). Interestingly, a 5%

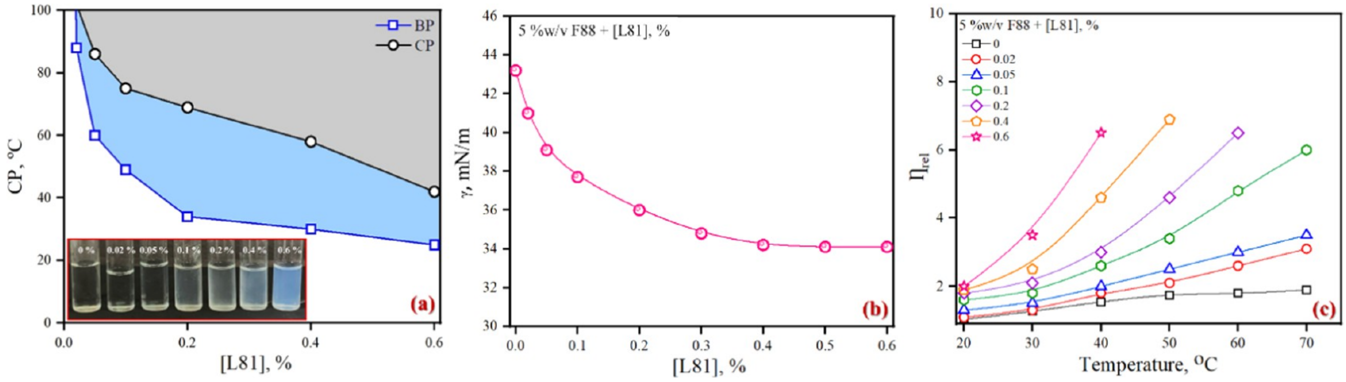

Figure 1. (a) Clouding behavior; (b) γ profile of 5% w/v F88 in varying [L81] at 30 °C; and (c) solution viscosity (η_{rel}) trend depicting the impact of [L81] on 5% w/v F88 as a function of temperature.

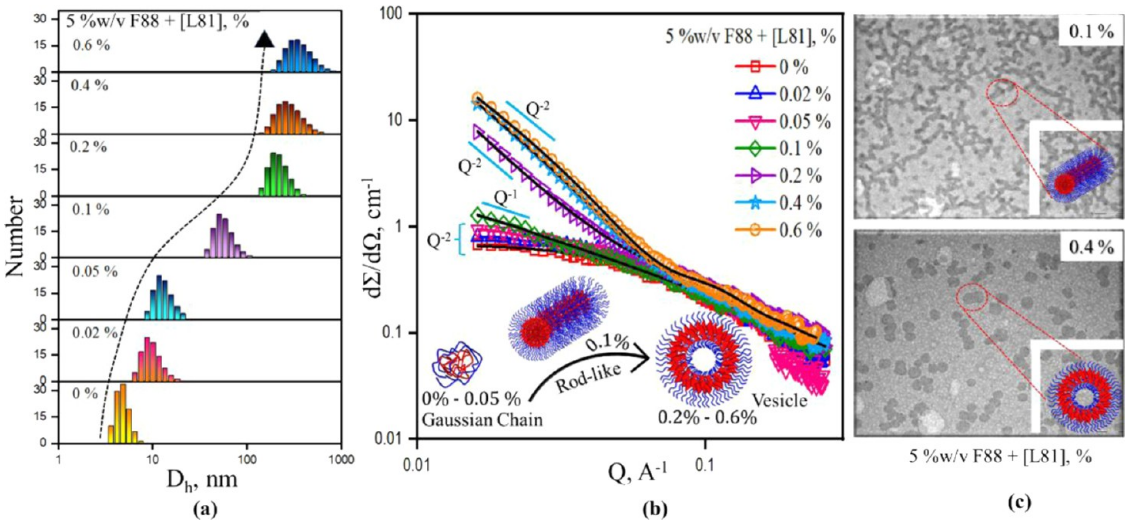

Figure 2. (a) Hydrodynamic diameter (D_h) distribution profile and (b) normalized scattering cross-sectional profile ($d\sum/d\Omega$) as a function of the scattering vector Q for different concentrations of L81 in 5% w/v F88 aqueous solution at 30 °C (solid lines represent the best fit with the model used). (c) TEM images represent the micellar morphology of 0.1 and 0.4% L81 in 5% w/v F88 with a scale bar of 1 μm.

w/v F88 solution in the presence of 0.4−0.6% L81 yields a bluish solution (inset vial images in the figure), which suggests a probable hint of micelle growth or morphology transition from spherical-to-rod-like micelles or vesicles, as reported in the published work.[35,39] The surface activity of any BCP is crucial for defining its industrial applications.[8,14,19,29] The surface tension (γ) of F88 solutions with varying L81 concentrations is plotted as the copolymer bulk concentration versus γ at 30 °C (Figure 1b). In the presence of a low L81 concentration, γ decreases, which is in good agreement with the Gibbs adsorption isotherm. Such a decrease in γ indicates favorable copolymer adsorption at the air−solution interface. The initial decrease of γ is followed by an abrupt change in the slope of γ with a change in the L81 concentration. Later, γ did not change or remained almost constant, suggesting the formation of micelles due to enhanced hydrophobic interactions between the polymeric chains.

According to the literature, CP and relative viscosity (η_{rel}) are closely related.[7,26,36] Hence, the effect of temperature on η_{rel}, both with and without L81, can be seen in Figure 1c. η_{rel} of 5% w/v F88 increased monotonically with increasing L81 concentration, and this trend strongly indicates the possibility of micellar growth/transition, further corroborated through scattering experiments.

Scattering Conduct. The hydrodynamic diameter (D_h) pattern obtained throughout the diffusion coefficient of 5% w/v F88 in aqueous solution at 30 °C is shown in Figure 2a. This solution showed a very weak scattering profile with a peak at around ∼4.7 nm denoting the presence of unimers. The addition of L81 promoted a gradual shift in the peaks that inferred micellar growth/transition. Such a trend is further examined by neutron scattering experiments following the use of various combinations of a hard-sphere structure factor and a core−corona hard-sphere form factor as discussed below. The solid lines in Figure 2b represent the fits to the scattering data, employed to determine the morphological parameters of the micelles using various models. The SANS data showed a Gaussian chain form factor utilizing eq 3 at 0.01 and 0.02% L81 in 5% w/v F88, respectively. A sharp correlation peak was observed with an increase in scattering intensity, indicating an increase in the population of unimers (Figure 2b). Rod-like micellar geometry was also determined, fitted using eq 5 with a slope of −1, at 0.1% L81, as depicted in Figure 2 and detailed in Table 1.

Gaussian chains with a radius of gyration (R_g) of ∼ 24.7 Å were observed in the 5% w/v F88 aqueous solution at 30 °C with a CMT of 35.9 °C (Table 1). The self-assembly of these unimers promotes the formation of micelles when the

Table 1. Fitted SANS Parameters for 5% w/v F88 Solution with Increasing Concentrations of L81 at 30 °C[a]

5% w/v F88 + [L81], %	size, Å	shape
0	$R_g = 24.7 \pm 0.3$	Gaussian chain
0.02	$R_g = 24.8 \pm 0.3$	Gaussian chain
0.05	$R_g = 27.8 \pm 0.4$	Gaussian chain
0.1	$R_{cr} = 10.4 \pm 0.2$; $L > 350$	rod-like micelle
0.2	$t_v = 83.9 \pm 0.9$; $R_v > 350$	vesicle
0.4	$t_v = 78.5 \pm 0.8$; $R_v > 350$	vesicle
0.6	$t_v = 77.4 \pm 0.8$; $R_v > 350$	vesicle

[a]Note: R_g = radius of gyration, R_{cr} = cross-sectional radius of rod-like micelles, L = length of rod-like micelles, R_v = radius of the vesicle, and t_v = thickness of the vesicle.

temperature increases with increasing PPO and PEO groups forming the micelle core and corona, respectively. The SANS data for 5% w/v F88 when varying the L81 concentration at 30 °C is shown in Figure 2b. The scattering intensity in the low-Q regime significantly increases when the L81 concentration is increased, indicating the presence of F88 micelles. This behavior corresponds with the interparticle structural factor that explains the large correlation peaks in the SANS in the presence of L81. Initially, no prominent changes were observed with the addition of 0.02 and 0.05% L81. This behavior resembles that of a 5% w/v F88 solution, specifically exhibiting a Gaussian chain form factor described by eq 5 with a slope of −2, resulting in an increase in R_g from 24.8 to 27.8 Å. This increase suggests a higher population of unimers. The Gaussian chains directly turned into rod-like micelles at 0.1% L81 with a cross-sectional radius of R_{cr} = 10.4 Å and a length of a rod-like micelle, L > 350 Å. This transition was modeled using eq 5 with a slope of −1. Such rod-like micelles are likely responsible for the observed increase in the viscosity of 0.1% L81 in comparison to lower concentrations, as illustrated in Figure 2c. Furthermore, an increase in scattering intensity, accompanied by a sharp correlation peak observed in Figure 2b, suggests an increase in the aggregation of micelles, i.e., vesicles were found (evaluated using eq 6) with a slope of −2 with increasing concentration of L81 from 0.2 to 0.6% L81. The same is evident in the TEM images in Figure 2c.

CG-MD Simulations. Two CG-MD simulations for aqueous solutions of F88 and L81 at concentrations of 5 wt %/v and 30 °C were carried out. Figure 3a shows the CG-MD simulation snapshots obtained after 8000 ns, indicating that small F68 spherical micelles with PEO groups were well solvated. The micelle density profile (shown on the right) denotes the arrangement of the PPO groups in the micelle core, whereas the PEO groups in orange form the micelle corona. The density profile also shows some PEO groups in the center of the micelle, which corresponds to the PEO belonging to neighboring micelles (cross-linkage). This indicates that the relatively large and well-solvated PEO branches can enhance the intermicelle interactions. Four micelles, with an aggregation number of N_{agg} ∼ 7, were obtained besides a few isolated F88 unimers. This is in contrast to experiments, in which only F88 unimers were found. Two

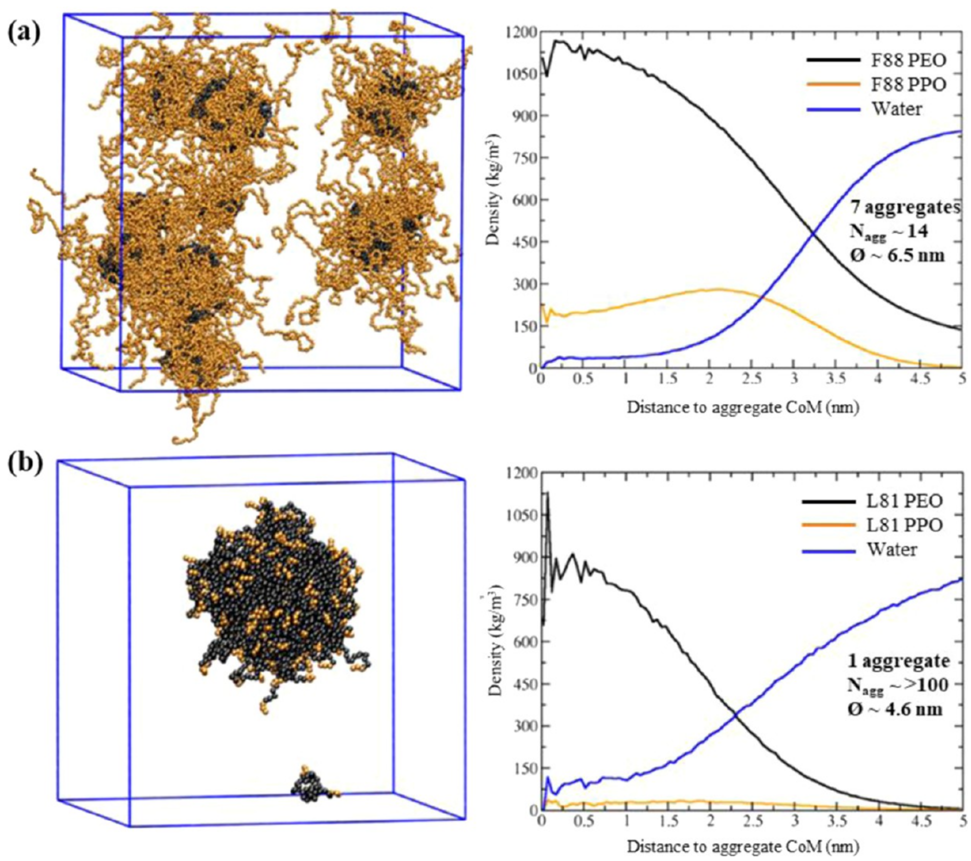

Figure 3. CG-MD simulation snapshot for (a) 5% w/v F88 and (b) 5% w/v L81 in aqueous solution at 30 °C. Density profiles, shown on the right, were obtained from the micelle center of mass (CoM). The color code is the same as that in Scheme 2 and water is shown in blue in the density profiles, whereas in the simulation, snapshots were removed for clarity.

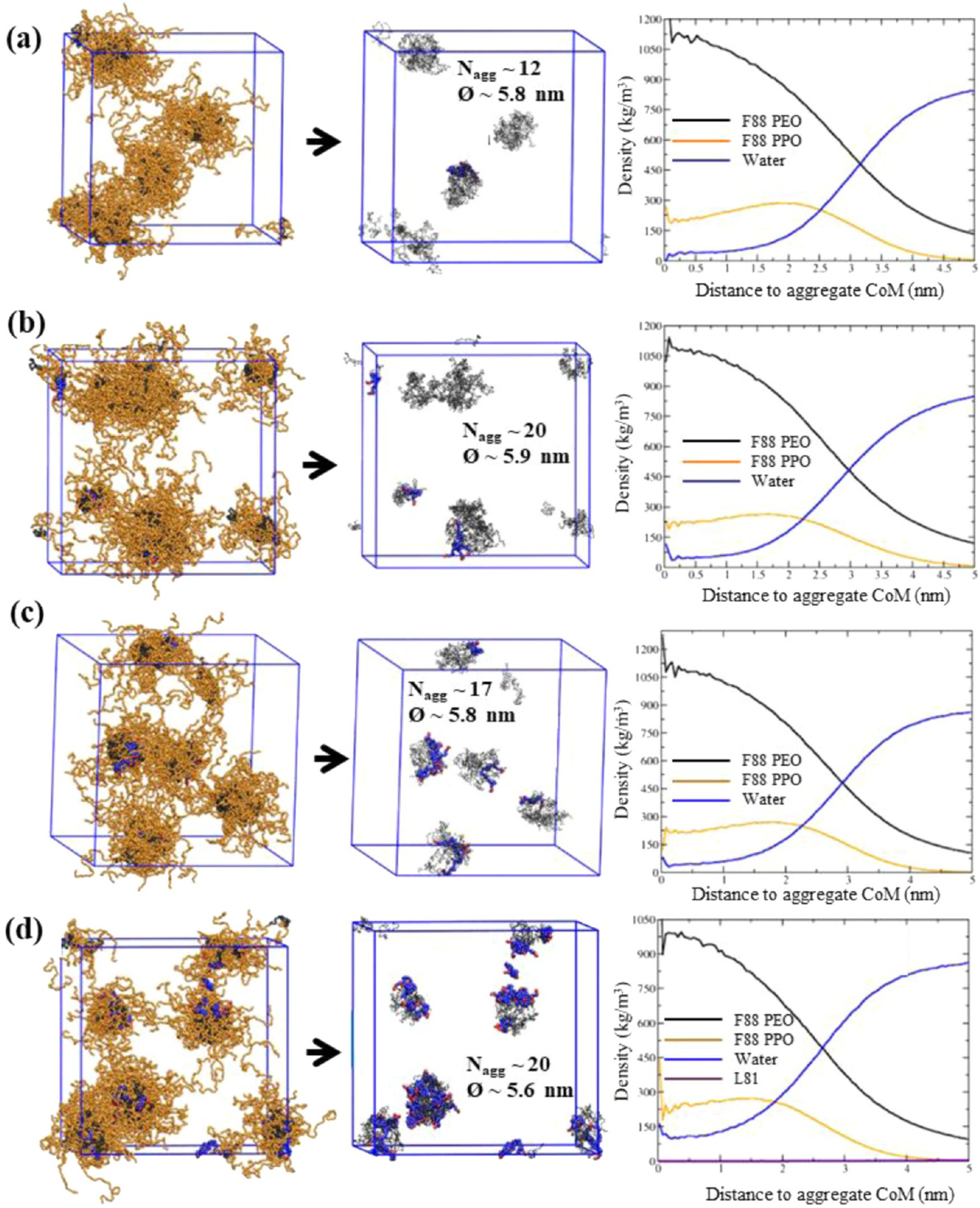

Figure 4. CG-MD simulation snapshots for 5% w/v F88 aqueous solutions with (a) 0.02%v/w, (b) 0.05% v/w, (c) 0.1% v/w, and (d) 0.4% v/w L81 at 30 °C. The color code follows that in Figure 3, but the L81 PPO and PEO groups are colored in blue and red, respectively. The density profiles for L81 could not be obtained due to the limitations of the cluster counting code in detecting the L81 moieties at such low concentrations.

factors could come into play: the fact that CG models have a tendency to overaggregate, whereas approximations taken in the experimental setups could miss the presence of small aggregates.

https://doi.org/10.1021/acs.jpcb.4c00561
J. Phys. Chem. B XXXX, XXX, XXX−XXX

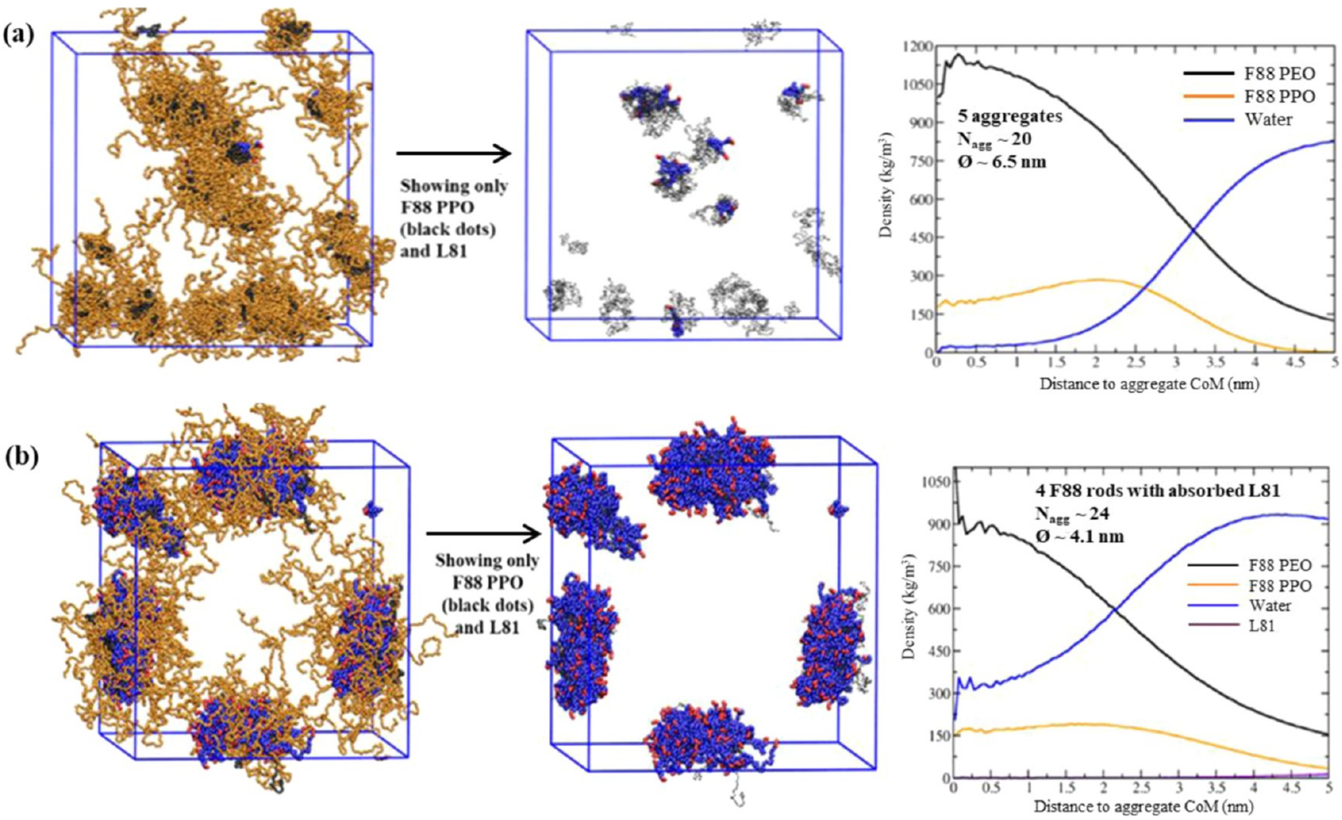

Figure 5. CG-MD simulation snapshots, with the density profiles focused on the micelle surface, for the 5% w/v F88 aqueous solution with (a) 0.1%v/w at 60 °C and (b) 4% v/w of L81 at 30 °C. The color code follows that in Figure 4.

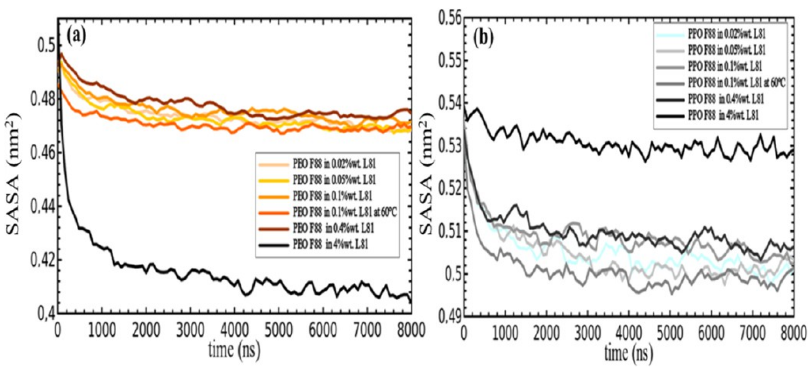

Figure 6. Solvent-accessible surface areas (SASA) for F88 (a) PEO and (b) PPO groups at a simulation time of 8000 ns denoting the impact of the L81 concentration and temperature on their level of hydration.

The L81 aqueous solution displayed a clearer scenario with the formation of a large aggregate, as shown in Figure 3b, owing to the hydrophobic character of L81. The density profile suggests that spherical shapes prevail, as also noticed by the homogeneous distribution of PEO along the surface. Since the PEO/PPO ratio in L81 is very low, some PEO groups can be found well inside the core region (CoM < 0.25 nm), suggesting that some L81 moieties can be arranged with the hydrophilic PEO groups pointing toward the micelle core. This simulation was carried out with 100 L81 moieties; thus, N_{agg} > 100, and the diameter (taken as the value of the maximum of the PEO density profile) was Ø ∼ 4.5 nm.

Figure 4 shows the CG-MD simulation snapshots for the 5% v/w F88 aqueous solution mixed with different concentrations of L81 at 30 °C. From a qualitative point of view, an increased number of L81 moieties absorbed by F88 small micelles was observed for solutions with 0.02, 0.05, and 0.1% L81, as shown in Figure 4a−c. Their micelle density profiles indicated a slight increase of the F88 aggregate size when the L81 concentration increased as a result of the absorbed L81. Quantitative analysis using the cluster counting code indicated F88 micelles with N_{agg} ∼ 12 and 20 at 0.02 and 0.05% L81 concentrations, respectively. Thus, a weak impact of L81 below 0.1% concentration was observed in the simulations, where the aggregates exhibited similar diameters of ∼5.9 nm. The solution with 0.1% v/w L81 yielded spherical aggregates in contrast to the rods observed in the experiments. In this regard, the simulation time was extended for another 8000 ns of simulation time, but the spherical structures persisted. Perhaps, a further increase of the simulation time could yield the expected sphere-to-rod transition observed in the experiments, but it is out of our computational capacities.

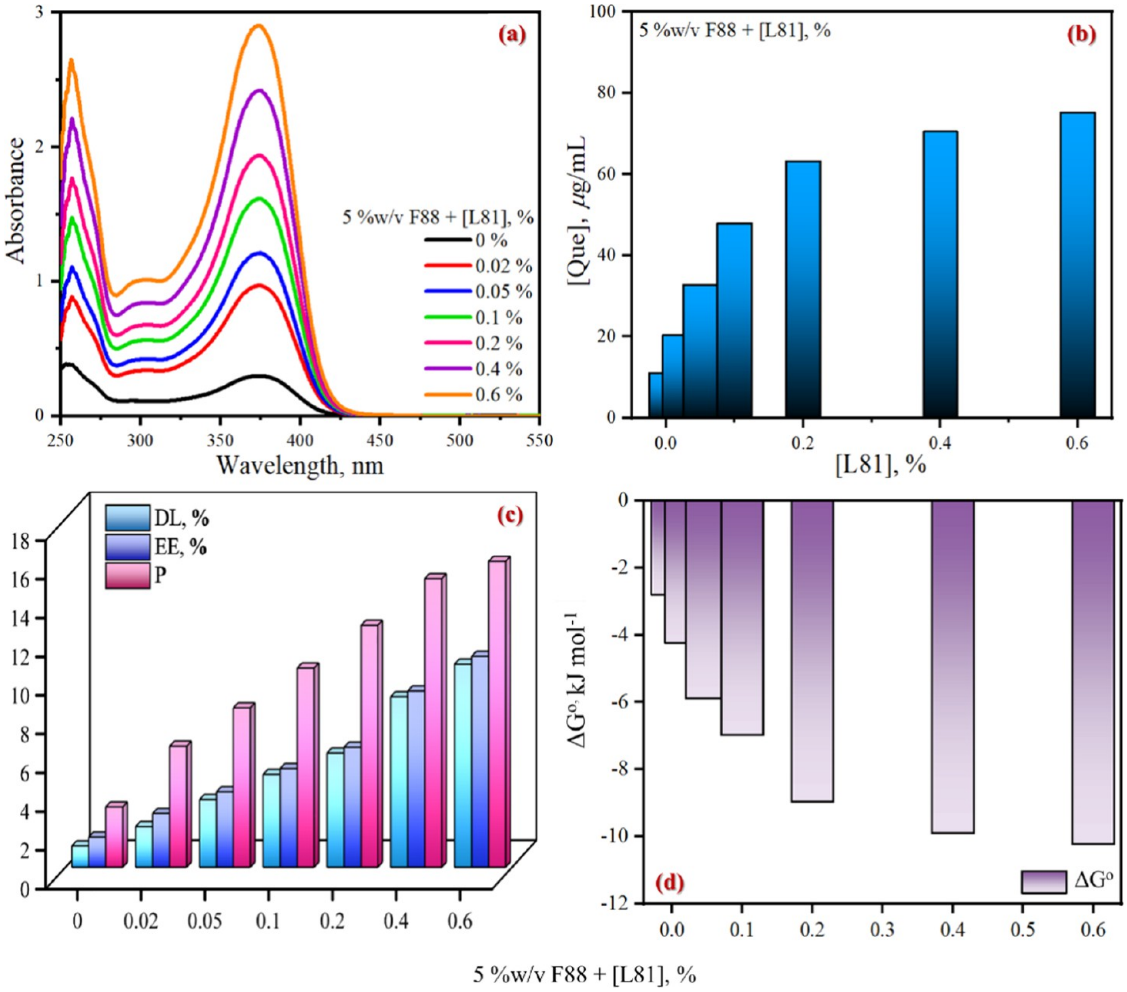

Figure 7. (a) Qualitative, (b) quantitative, (c) drug-loading (DL, %), encapsulating efficiency (EE, %), partition coefficient (P), and (d) Gibbs energy for QCT solubilized in 5 wt %/v F88 with increasing concentrations of L81.

Figure 4d shows the solution with increased L81 (0.4%), also exhibiting spherical aggregates; however, the density profiles denoted the presence of PEO and water in the F88 micelle core (CoM < 0.25 nm), indicating a plausible formation of early vesicles. In this solution, the increased absorption of L81 somehow disrupted the micelle core, facilitating the arrangement of F88 inside the micelle core besides some water molecules.

Two additional simulations were developed: the solution, shown in Figure 4c, but at 60 °C to speed up the dynamics and facilitate any plausible phase transition besides an increase of four times in the concentration of L81 of the solution, as shown in Figure 4d. However, spherical aggregates remained even for simulations up to 16,000 ns of simulation time, as shown in Figure 5a. The density profile also indicated spherical shapes. Encouragingly, when the concentration of L81 was increased to 4%, prolate-shaped structures were observed at 30 °C, as shown in Figure 5b. These were the initial stages of micellar rod formation observed in the experiments. The density profile was flattened, reinforcing the presence of prolate micelles. This highlights the fact that CG-MD simulations could not capture the impact of L81 at low concentrations, and only when the concentration of L81 was noticeably increased could a reasonable agreement with the experimental results be found.

Figure 6 shows the SASA profiles of the PEO and PPO groups of F88 when L81 was added at a simulation time of 8000 ns. The SASA of the PEO F88 groups in Figure 6a denotes a slight dehydration process of the F88 micelle coronas when the L81 concentration is increased from 0.02 to 0.1% at 30 °C. The increased number of L81 moieties absorbed by the F88 micelles generated a barrier for the PEO F88 groups to remain in contact with water. This dehydration was more evident when the temperature was increased from 30 to 60 °C in the solution with 0.1% L81. A slight increase in the F88 PEO hydration was noticed at 0.4% L81 (brown line), indicating some changes in the structure of the F88 micelles. This could correspond to the formation of early vesicles, as pointed out earlier in the density profile (Figure 4d). When 4% L81 was added, the dehydration of F88 PEO groups was more noticeable, highlighting the fact that the increased amount of absorbed L81 moieties shielded the F88 PEO groups from the water environment. The increased concentration of L81 at the F88 micelle surface could be the smoking gun behind the sphere-to-rod transition observed in the experiments, as noted in the simulation snapshots in Figure 5b. Therefore, L81 disrupted the equilibrium of the PEO−PEO interactions at the F88 micelle surface, promoting more energetically favorable flattened surfaces. Likewise, Figure 6b displays the level of hydration of PPO groups of F88, indicating similar dehydration when the concentration of L81 was increased.

https://doi.org/10.1021/acs.jpcb.4c00561
J. Phys. Chem. B XXXX, XXX, XXX−XXX

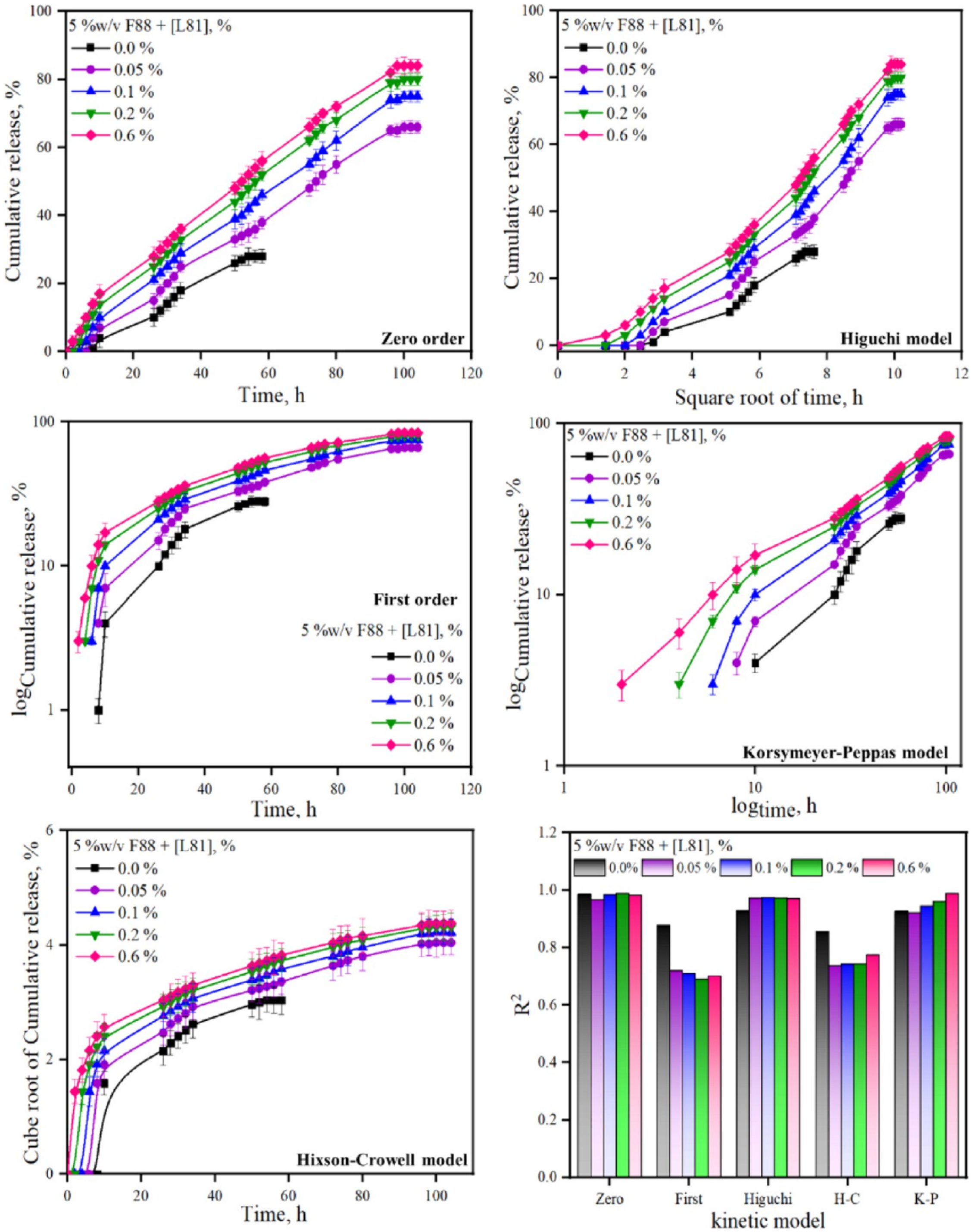

Figure 8. Different kinetic models for the in vitro QCT release profile from 5 wt %/v F88 and the impact of L81. (the solid lines and equations represent the best fit with the model used, which reveals the drug release from the micelle, where Q_0 = initial amount of the drug; Q_t = cumulative amount of drug at time "t"; t = time in hours; k = release constant).

Likewise, in PEO F88 groups, when the temperature was raised (30−60 °C), the solution with 0.1% L81 showed slight PPO dehydration of F88 micelles. Noticeable PPO F88 hydration was observed in the solution with 4% L81, reinforcing the above-mentioned transition of F88 to flattened structures. The formation of a prolate-shaped F88 micelle configuration facilitates the access of water to the F88 PPO groups when compared with the spherical micellar configurations.

Spectral Validation. A major challenge in pharmaceutics is creating effective block copolymeric-based formulations that can efficiently deliver hydrophobic drugs since they entail outstanding biocompatibility, especially remarkable drug-loading capacities, and excellent chemical and thermal stability when compared with other nanocarriers.[73,73] Hence, in this direction literature studies have the key role of illustrating hydrophobic and electrostatic interactions that induce nano-scale self-assembly and impact drug-loading/release properties.[13,17,70]

The solubility and release interest employing F88/L81 micelles were focused on the hydrophobic drug quercetin

https://doi.org/10.1021/acs.jpcb.4c00561
J. Phys. Chem. B XXXX, XXX, XXX−XXX

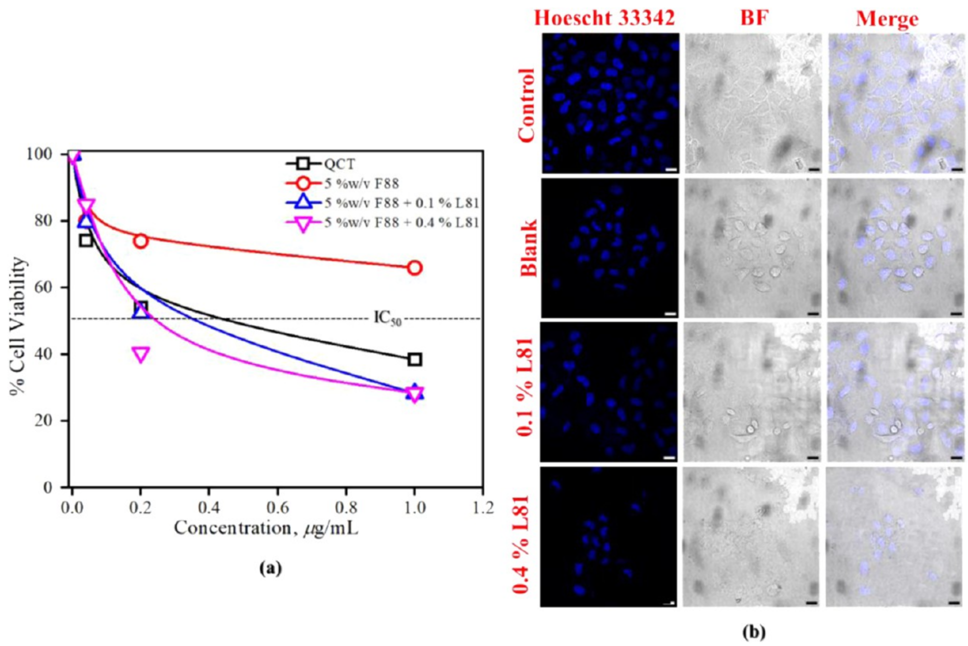

Figure 9. (a) Concentration−cell viability (dose−response) profile of HeLa cells exposed to the QCT-loaded BCP mixture for 12 h; and (b) bright-field and fluorescence microscopic images of HeLa cells after 1 h of cellular uptake with control and QCT-loaded micelles.

(QCT) due to its wide range of pharmacological applications, including anti-inflammatory, antioxidant, and anticancer effects.[7,39,73]

Figure 7a displays the broad QCT spectra with the absorbance maxima recorded at ∼369 nm, which is induced by the low-energy $\pi-\pi^*$ excitation, consistent with the published data.[7,26,35,69] The amount of QCT absorbed in 5% w/v F88 without L81 is 11 μg/mL, which is higher than the poor solubility of QCT in water (∼0.4 μg/mL). Also, due to the absence of micelles, the QCT remained poorly soluble in a 5% w/v F88 solution, but solubility enhancement was observed with the addition of L81. As previously described, the addition of L81 promoted F88 self-assembly and micelle growth, thereby enhancing QCT solubilization, as shown in Figure 7a,b.

Increased QCT solubilization manifested in terms of drug loading (DL%) and encapsulation efficiency (EE %). The results of QCT solubilization in 5% w/v F88 with and without L81 (blank) illustrate the impact of a suitable BCP choice, as shown in Figure 7c. Here, it is assumed that QCT is hydrophobic, and a significant portion of QCT can be preferentially found in the hydrophobic PPO core rather than in the hydrophilic PEO micelle corona.[49] The higher DL % observed for 0.6% L81 in 5 wt %/v F88 suggests that QCT was encapsulated in the inner core of the micelle and interacted with the hydrophobic domain. Additionally, previous studies have indicated an inverse correlation between the %PEO units and the drug encapsulation ability.[7,13] Thus, fine-tuning of the BCP composition can enhance DL% and stability. In addition, the partition coefficient (P) was further calculated by comparing the solubility of QCT in the presence of the F88/L81 micellar phase with its solubility in water. The presence of L81 resulted in a significant increase of P values compared with the 5% w/v F88 (blank) solution. This indicates an affinity of QCT for this system due to a more favorable hydrophobic environment that enhances solubilization.[26] From a thermodynamic point of view, a more negative ΔG° yields a more favorable process. Thus, it can be inferred that the incorporation of QCT in the blended system showing solubilization enhancement is more thermodynamically favorable than the 5% w/v F88 (blank) solution, as shown in Figure 7d.

Release Kinetics. Studies have illustrated that the compatibility between a drug and BCP determines its favorable degree of solubility, whereas the location of the drug in the BCP micelle determines its release.[13,17,44,46] Also, the length of the PPO and PEO blocks in BCPs determines the effectiveness of the QCT loading/releasing processes. Thus, our study aims to analyze the loading capacity and release kinetics of QCT in a blended system. Over the past few decades, numerous drug delivery approaches have been attempted,[39] including mathematical models that aim to describe load/release mechanisms to improve their efficiency. However, it is not always clear which mathematical theory underlies the complexity of the chemical and physical processes involved. In fact, to find a proper transport mechanism for QCT release from the blended copolymeric systems, several kinetic models were employed and the data was fitted accordingly, as described in Figure 8.

Based on the R^2 value, it can be stated that the Higuchi model is superior in its ability to capture the release profile of QCT. Diffusion from the blended Pluronic system is responsible for regulating the release of QCT. The presence of L81 micelles facilitated the regulated release of QCT in the nanocarrier system that contained a weight-to-volume percentage of F88. The findings of this study suggest that QCT-loaded blended micelles can effectively deliver drugs. The information provided here highlights the significance of this research and generates the potential applications of such a nanocarrier system for controlled drug release.

Cellular Uptake and Cytotoxicity Assay. The therapeutic utilization of hydrophobic drugs is often hindered by their poor solubility and bioavailability.[36,39,69−74] In our study, we encountered this challenge with QCT, which suffers from

https://doi.org/10.1021/acs.jpcb.4c00561
J. Phys. Chem. B XXXX, XXX, XXX−XXX

poor bioavailability and requires an appropriate carrier to overcome these obstacles while maintaining its efficacy. Literature extensively supports the potential of QCT to induce apoptosis in various tumor tissues.[75] Hence, we carried out the cytotoxic analysis in the examined system in HeLa cells, as illustrated in Figure 9a.

The MTT assay was performed on HeLa cells treated with QCT encapsulated in various F88 micelles for 12 h. The limited water solubility of QCT yielded insufficient dissolution in the cell medium, resulting in precipitation and subsequent reduction in the duration of effective cell exposure to release QCT.[49] Therefore, cells were less susceptible to cytotoxicity by QCT solutions than by QCT-loaded blended micelles (5 wt %/v F88) (Figure 9a). Up to 60% of cells were viable at 0.2 μg/mL QCT-loaded F88 micelles. 0.1 and 0.4% L81 in 5% w/v F88 showed inhibition of cell viability in 12 h at 0.2 and 0.25 μg/mL, respectively (Figure 9). The IC_{50} value, which represents the concentration at which 50% of cells were killed, was determined for each system. The difference in the IC_{50} value of QCT might be due to the different types of BCP involved and their ability to release the QCT inside the cell.[76−78] The cytostatic abilities of BCP micelles are responsible for their higher cytotoxicity.[76−78] Specifically, very hydrophobic copolymers, such as the L81 (0.1 and 0.4%), exhibited IC_{50} values of 0.2 and 0.245 μg/mL, respectively. On the other hand, highly hydrophilic copolymers, like F88, exhibited less toxic effects and were unable to eliminate 50% of the cells.

Untreated cells were used as controls in this study. Upon treating the cells with 0.1 and 0.4% of L81, we observed a noticeable change in the cell morphology, as shown in Figure 9b. This can be attributed to the limited water solubility of the compounds, leading to their precipitation and consequently reducing the effective exposure time of free QCT within the treated cells. As a result, the cytotoxicity was compared to that of cells treated with QCT-loaded F88 micelles, as depicted in Figure 9b. Additionally, as the dosage increased, we observed a decrease in cancer cell viability, indicating enhanced cytotoxicity, which can be attributed to the successful solubilization of QCT in the F88 micelles. This result suggests that the encapsulation of QCT within F88 and the nontoxic nature of F88 contributed to the observed outcomes, as depicted in Figure 9b. Thus, we can conclude that QCT-loaded micelles have a significant impact on HeLa cells due to the increased solubility of QCT, which is attributed to their large size and unique morphology.

■ CONCLUSIONS

Our study illustrates the impact of hydrophobic BCP L81 in inducing the micellization of F88 in an aqueous solution. Careful analysis of the phase behavior of F88 revealed that the addition of L81 induced a decrease in the CP of 5% w/v F88 aqueous solutions (>100 °C in water). The surface tension (γ) of the F88 solution decreases in the presence of the L81. Here, micelle formation was observed to be primarily driven by hydrophobic interactions. The more hydrophilic the F88, the greater the water that must be replaced from the micellar core and corona with the addition of L81 due to increased hydrophobicity. The shift in the solution viscosity (η_{rel}) promoted a probable hint of micellar growth/transition in the BCP micelles. Micelle size distributions were determined from scattering experiments. Here, detailed structural information at various stages of self-assembly, such as the size of the core and corona and the volume fraction of the micelles, was obtained from SANS. L81 promotes F88 micellization by competing for hydrogen bonding with water molecules to modify the solvent quality, thereby leading to a reduction in the solubility of both the PPO and PEO segments of F88. The addition of L81 to F88 increased the aggregation and enhanced the core radius. The obtained experimental results were confirmed by coarse-grained molecular dynamics simulations. The micelle distribution of the 5% w/v F88 aqueous solution and the impact of L81 addition were characterized and compared with the experimental results. The 5% w/v F88 aqueous solution formed small aggregates in equilibrium with the unimers. An increase in F88 self-assembly was observed as soon as L81 was added. The size of the F88 aggregates barely increased when small amounts of L81 were added. Simulation snapshots showed how the L81 moieties were absorbed by the F88 aggregates and distributed on the surface. Above a certain L81 concentration (∼0.1%), early vesicle formation was observed, as confirmed by the micelle density profiles, and was in good agreement with our experimental results. SASA provided a more detailed scenario for the PEO and PPO groups of F88 to characterize their hydration/dehydration properties when L81 was added. SASA profiles along the simulation showed that the F88 micelle coronas were barely dehydrated when a small amount of L81 was added (<0.1% at 30 °C) but was more evident when the temperature was increased. Above this L81 concentration, some changes were observed in the structure of the F88 micelles compatible with the formation of small vesicles. With a further increase of L81 (4%), the dehydration of the F88 micelle corona was more evident, favored by the increased L81 moieties, which hindered the interactions between water and the F88 micelle corona. In fact, the SASA of the F88 corona dramatically decreased when 4%v/w was added to the solution. Therefore, the increased L81 around the F88 micelle surface somehow disrupted the F88 PEO−PEO interactions at the micelle surface, promoting the formation of more energetically favorable flattened structures. As such, the combination of our experimental results with MD simulations offers a thorough understanding of the behavior of nanoscale micellization in the studied mixed systems. UV studies showed that more drugs could be accommodated in the host micelles of mixed Pluronic than in the single micelles of hydrophilic F88. To determine how the hydrophobic interactions would impact the QCT release, the release from 5% w/v F88 was investigated. The mechanism of QCT release was clarified through data fitting using a variety of mathematical kinetic models, and the results showed that the Higuchi model provided the best match, suggesting that the diffusion process could be used to control drug release. Furthermore, by carefully choosing the sample ratios and considering the development of micellar geometries, these templates were successfully used to solubilize QCT in HeLa cells in in vitro experiments, which showed encouraging cytotoxic effects. Thus, this study emphasizes the potential of BCP combinations to influence cancer cell viability, which opens exciting possibilities for the creation of chemically stable nanoscale blends that can be used in the pharmaceutical industry.

■ AUTHOR INFORMATION

Corresponding Author

Ketan Kuperkar − *Department of Chemistry, Sardar Vallabhbhai National Institute of Technology (SVNIT),* Surat 395 007 Gujarat, India; orcid.org/0000-0001-8039-9012; Email: ketankuperkar@gmail.com

Authors

Divya Patel − *Department of Chemistry, Sardar Vallabhbhai National Institute of Technology (SVNIT), Surat 395 007 Gujarat, India*

Nitumani Tripathi − *Department of Chemistry, Sardar Vallabhbhai National Institute of Technology (SVNIT), Surat 395 007 Gujarat, India*

Payal Vaswani − *Biomedical Engineering, Indian Institute of Technology Gandhinagar (IITGn), Gandhinagar 382 355 Gujarat, India*

Germán Pérez-Sánchez − *CICECO − Aveiro Institute of Materials, Department of Chemistry, University of Aveiro, Aveiro 3810-1933, Portugal;* orcid.org/0000-0002-3972-5901

Dhiraj Bhatia − *Biomedical Engineering, Indian Institute of Technology Gandhinagar (IITGn), Gandhinagar 382 355 Gujarat, India;* orcid.org/0000-0002-1478-6417

João A. P. Coutinho − *CICECO − Aveiro Institute of Materials, Department of Chemistry, University of Aveiro, Aveiro 3810-1933, Portugal;* orcid.org/0000-0002-3841-743X

Pratap Bahadur − *Department of Chemistry, Veer Narmad South Gujarat University (VNSGU), Surat 395 007 Gujarat, India*

Complete contact information is available at: https://pubs.acs.org/10.1021/acs.jpcb.4c00561

Author Contributions

D.P., Ni.T., and P.V. performed the experimental work. G.P.-S., D.B., and K.K. were responsible for analyzing the experimental data and writing the paper. J.A.P.C. and P.B. directed this research. All authors approved the manuscript.

Notes

Ethics Statement: No human or animal subjects were used in this research.

Declaration of Generative AI and AI-Assisted Technologies in the Writing Process: During the preparation of this work, the authors used Chat GPT TOOL/SERVICE in order to rephrase several statements in the manuscript. After using this tool/service, the authors reviewed and edited the content as needed and take full responsibility for the content of the publication.

The authors declare no competing financial interest.

■ ACKNOWLEDGMENTS

The authors acknowledge the Sardar Vallabhbhai National Institute of Technology (SVNIT), Gujarat, India, for providing instrumentation facilities. The authors also acknowledge the scattering experiments support from the Solid State Physics Division, Bhabha Atomic Research Centre (BARC), Mumbai, India. The authors also acknowledge Arash Elahi (Department of Chemical Engineering at the University of Illinois at Chicago, USA) for kindly providing the MD computer simulation input files for the Pluronic molecules used in this work. The computational part of this work was funded by the CICECO-Aveiro Institute of Materials under the projects UIDB/50011/2020, UIDP/50011/2020, and LA/P/0006/2020 and financed by national funds through the FCT/MEC (PIDDAC. Germán Pérez-Sánchez acknowledges the national funds (OE), ref DL 57/2016/CP1482/CT004 and DOI: 10.54499/DL57/2016/CP1482/CT0043 through FCT—Fundação para a Ciência e a Tecnologia, I.P., in the scope of the framework contract foreseen in numbers 4, 5, and 6 of the articles 23, of the Decree-Law 57/2016, of August 29, changed by Law 57/2017, of July 19. Simulations were performed at the OBLIVION Supercomputer managed by the HPC Centre of the University of Évora and acquired under the "Enabling Green E-science for the SKA Research Infrastructure (ENGAGE SKA)", reference POCI-01-0145-FEDER-022217, funded by COMPETE 2020 and the Foundation for Science and Technology (FCT), Portugal. No specific grants were received from any funding agencies in the public, commercial, or not-for-profit sectors for the experiments. Simulations were financed by the FCT program "Concurso de Projetos de Computação Avançada -3a Edição" with the project reference CPCA/A2/15575/2022.

■ REFERENCES

(1) Chiappetta, D. A.; Sosnik, A. Poly(ethylene oxide)−poly(propylene oxide) block copolymer micelles as drug delivery agents: Improved hydrosolubility, stability and bioavailability of drugs. *Eur. J. Pharm. Biopharm.* **2007**, *66*, 303−317.

(2) Zarrintaj, P.; Ramsey, J. D.; Samadi, A.; Atoufi, Z.; Yazdi, M. K.; Ganjali, M. R.; Amirabad, L. M.; Zangene, E.; Farokhi; Thomas, S.; et al. Poloxamer: A versatile tri-block copolymer for biomedical applications. *Acta Biomater.* **2020**, *110*, 37−67.

(3) Kabanov, A. V.; Batrakova, E. V.; Alakhov, V. Yu. Pluronic block copolymers as novel polymer therapeutics for drug and gene delivery. *J. Controlled Release* **2002**, *82*, 189−212.

(4) Rey-Rico, A.; Cucchiarini, M. PEO-PPO-PEO Tri-Block Copolymers for Gene Delivery Applications in Human Regenerative Medicine. *Int. J. Mol. Sci.* **2018**, *19*, 775−790.

(5) Karayianni, M.; Pispas, S. Block copolymer solution self-assembly: Recent advances, emerging trends, and applications. *J. Polym. Sci.* **2021**, *59*, 1874−1898.

(6) Rahdar, A.; Kazemi, S.; Askari, F. Pluronic as nano-carrier platform for drug delivery systems. *Nanomed. Res. J.* **2018**, *3*, 174−179, DOI: 10.22034/nmrj.2018.04.001.

(7) Patel, D.; Ray, D.; Aswal, V. K.; Kuperkar, K.; Bahadur, P. Micellar assembly leading to structural growth/transition in normal and reverse Tetronics in single and mixed solution environment. *Soft Matter* **2022**, *18*, 4543−4553.

(8) Alexander, S.; Cosgrove, T.; Castle, T. C.; Grillo, I.; Prescott, S. W. Effect of Temperature, Cosolvent, and Added Drug on Pluronic-Flurbiprofen Micellization. *J. Phys. Chem. B* **2012**, *116*, 11545−11551.

(9) Kwon, G. S. Polymeric micelles for delivery of poorly water-soluble compounds. *Crit. Rev. Ther. Drug Carr. Syst.* **2003**, *20*, 357−403.

(10) Tiwari, S.; Kansara, V.; Bahadur, P. Targeting Anticancer Drugs with Pluronic Aggregates: Recent Updates. *Int. J. Pharm.* **2020**, *586*, 119544−119588.

(11) Karimi, M.; Sahandi Zangabad, P.; Ghasemi, A.; Amiri, M.; Bahrami, M.; Malekzad, H.; Ghahramanzadeh Asl, H.; Mahdieh, Z.; Bozorgomid, M.; Hamblin, R.; et al. Temperature-Responsive Smart Nanocarriers for Delivery of Therapeutic Agents: Applications and Recent Advances. *ACS Appl. Mater. Interfaces.* **2016**, *8*, 21107−21133.

(12) Kuperkar, K.; Atanase, L. I.; Bahadur, A.; Crivei, I. C.; Bahadur, P. Degradable Polymeric Bio (nano) materials and Their Biomedical Applications: A Comprehensive Overview and Recent Updates. *Polymers* **2024**, *16*, 206−251.

(13) Tasca, E.; Andreozzi, P.; Del Giudice, A.; Galantini, L.; Schillén, K.; Giuliani, A. M.; de los Angeles Ramirez, M.; Moya, S. E.; Giustini, M. Poloxamer/sodium cholate co-formulation for micellar encapsulation of doxorubicin with high efficiency for intracellular delivery: An in-vitro bioavailability study. *J. Colloid Interface Sci.* **2020**, *579*, 551−561, DOI: 10.1016/j.jcis.2020.06.096.

(14) Bodratti, A. M.; Alexandridis, P. Formulation of Poloxamers for Drug Delivery. *J. Funct. Biomater.* **2018**, *9*, No. 11, DOI: 10.3390/jfb9010011.
(15) Batrakova, E. V.; Kabanov, A. V. Pluronic block copolymers: Evolution of drug delivery concept from inert nanocarriers to biological response modifiers. *J. Controlled Release* **2008**, *130*, 98−106.
(16) Vyas, B.; Pillai, S. A.; Bahadur, P. Influence of surfactant's polar head group charge on the self-assembly of three PEO−PPO−PEO triblock copolymers of widely varying hydrophobicity. *J. Mol. Liq.* **2020**, *316*, 113858−113869.
(17) Desiderio, L.; Gjerde, N. S.; Tasca, E.; Galantini, L.; Llarena, I.; Di Gianvincenzo, P.; Thongsom, S.; Moya, S. E.; Giustini, M. Determination of the optimal pH for doxorubicin encapsulation in polymeric micelles. *J. Colloid Interface Sci.* **2024**, *664*, 972−979.
(18) Mata, J. P.; Majhi, P. R.; Guo, C.; Liu, H. Z.; Bahadur, P. Concentration, temperature, and salt-induced micellization of a triblock copolymer Pluronic L64 in aqueous media. *J. Colloid Interface Sci.* **2005**, *292*, 548−556.
(19) Zhou, Z.; Chu, B. Light-scattering study on the association behavior of triblock polymers of ethylene oxide and propylene oxide in aqueous. *J. Colloid Interface Sci.* **1988**, *126*, 171−180.
(20) Naskar, B.; Ghosh, S.; Moulik, S. P. Solution Behavior of Normal and Reverse Triblock Copolymers (Pluronic L44 and 10R5) Individually and in Binary Mixture. *Langmuir* **2012**, *28*, 7134−7146.
(21) Chiappetta, D. A.; Sosnik, A. Poly(ethylene oxide)-poly-(propylene oxide) block copolymer micelles as drug delivery agents: Improved hydrosolubility, stability and bioavailability of drugs. *Eur. J. Pharm. Biopharm.* **2007**, *66*, 303−317.
(22) Marinov, G.; Michels, B.; Zana, R. Study of the State of the Triblock Copolymer Poly(ethylene oxide)-Poly(propylene oxide)-Poly(ethylene oxide) L64 in Aqueous Solution. *Langmuir* **1998**, *14*, 2639−2644.
(23) Singh, P. K.; Kumbhakar, M.; Pal, H.; Nath, S. Modulation in the Solute Location in Block Copolymer-Surfactant Supramolecular Assembly: A Time-resolved Fluorescence Study. *J. Phys. Chem. B* **2009**, *113*, 1353−1359.
(24) Bharatiya, B.; Patel, K.; Song, H.; Ma, J. H.; Aswal, V. K.; Bahadur, P. Lipophilic Diol Induced Micellization of Pluronic F88 in Water. *J. Macromol. Sci., Part A* **2009**, *46*, 304−311.
(25) Jain, N. J.; Aswal, V. K.; Goyal, P. S.; Bahadur, P. Micellar Structure of an Ethylene Oxide-Propylene Oxide Block Copolymer: A Small-Angle Neutron Scattering Study. *J. Phys. Chem. B* **1998**, *102*, 8452−8458.
(26) Schillén, K.; Bryskhe, K.; Mel'nikova, Y. S. Vesicles formed from a poly (ethylene oxide)-poly (propylene oxide)-poly (ethylene oxide) triblock copolymer in dilute aqueous solution. *Macromolecules* **1999**, *32*, 6885−6888.
(27) Patel, D.; Kuperkar, K.; Yusa, S. I.; Bahadur, P. Nanoscale Self-Assemblies from Amphiphilic Block Copolymers as Proficient Templates in Drug Delivery. *Drugs Drug-Candidates* **2023**, *2*, 898−922.
(28) Rey-Rico, A.; Cucchiarini, M. PEO-PPO-PEO tri-block copolymers for gene delivery applications in human regenerative medicine-an overview. *Int. J. Mol. Sci.* **2018**, *19*, 775−790.
(29) Khimani, M.; Rao, U.; Bahadur, P. Calorimetric and Scattering Studies on Micellization of Pluronics in Aqueous Solutions: Effect of the Size of Hydrophilic PEO End Blocks, Temperature, and Added Salt. *J. Dispersion Sci. Technol.* **2014**, *35*, 1599−1610, DOI: 10.1080/01932691.2013.858349.
(30) Alexandridis, P.; Hatton, T. A. Poly(ethylene oxide)-poly-(propylene oxide)-poly (ethylene oxide) block copolymer surfactants in aqueous solutions and at interfaces: thermodynamics, structure, dynamics, and modelling. *Colloids Surf., A* **1995**, *96*, 1−46, DOI: 10.1016/0927-7757(94)03028-X.
(31) Verma, P.; Nath, S.; Singh, P. K.; M, K.; Pal, H. Effects of Block Size of Pluronic Polymers on the Water Structure in the Corona Region and Its Effect on the Electron Transfer Reactions. *J. Phys. Chem. B* **2008**, *112* (20), 6363−6372, DOI: 10.1021/jp711642x.
(32) Attia, A. B. E.; Ong, Z. Y.; Hedrick, J. L.; Lee, P. P.; Ee, P. L. R.; Hammond, P. T.; Yang, Y. Y. Mixed micelles self-assembled from block copolymers for drug delivery. *Curr. Opin. Colloid Interface Sci.* **2011**, *16*, 182−194, DOI: 10.1016/J.COCIS.2010.10.003.
(33) Senthilkumar, M.; Dash, S.; Vigneshwari, R.; Paulraj, E. Aceclofenac-loaded pluronic F108/L81 mixed polymeric micelles: effect of HLB on solubilization. *Des. Monomers Polym.* **2022**, *25*, 1−11.
(34) Zhao, Y.; Li, Y.; Ge, J.; Li, N.; Li, L. B. Pluronic-poly (acrylic acid)-cysteine/Pluronic L121 mixed micelles improve the oral bioavailability of paclitaxel. *Drug Dev. Ind. Pharm.* **2014**, *40*, 1483−1493.
(35) Manjappa, A. S.; Kumbhar, P. S.; Patil, A. B.; Disouza, J. I.; Patravale, V. B. Polymeric Mixed Micelles: Improving the Anticancer Efficacy of Single-Copolymer Micelles. *Crit. Rev. Ther. Drug Carrier Syst.* **2019**, *36*, 1−58.
(36) Patel, D.; Patel, D.; Ray, D.; Kuperkar, K.; Aswal, V. K.; Bahadur, P. Single and mixed Pluronics micelles with solubilized hydrophobic additives: Underscoring the aqueous solution demeanor and micellar transition. *J. Mol. Liq.* **2021**, *343*, 117625−117637.
(37) Oh, K. T.; Bronich, T. K.; Kabanov, A. V. Micellar formulations for drug delivery based on mixtures of hydrophobic and hydrophilic Pluronic block copolymers. *J. Controlled Release* **2004**, *94*, 411−422.
(38) Kulthe, S. S.; Inamdar, N. N.; Choudhari, Y. M.; Shirolikar, S. M.; Borde, L. C.; Mourya, V. K. Mixed micelle formation with hydrophobic and hydrophilic Pluronic block copolymers: implications for controlled and targeted drug delivery. *Colloids Surf., B* **2011**, *88*, 691−696.
(39) Patel, D.; Gawali, S. L.; Kuperkar, K.; Hassan, P. A.; Bahadur, P. Co-micellization conduct and structural dynamics of block copolymers in water and salt solution environment for drug solubilization enhancement. *Colloid Polym. Sci.* **2023**, *301*, 1−13, DOI: 10.1007/s00396-023-05109-x.
(40) Bhendale, M.; Singh, J. K. Molecular Insights on Morphology, Composition, and Stability of Mixed Micelles Formed by Ionic Surfactant and Nonionic Block Copolymer in Water Using Coarse-Grained Molecular Dynamics Simulations. *Langmuir* **2023**, *39*, 5031−5040.
(41) Albano, J. M. R.; Grillo, D.; Facelli, J. C.; Ferraro, M. B.; Pickholz, M. Study of the Lamellar and Micellar Phases of Pluronic F127: A Molecular Dynamics Approach. *Processes* **2019**, *7*, 606−617.
(42) Nie, S. Y.; Lin, W. J.; Yao, N.; Guo, X. D.; Zhang, L. J. Drug release from pH-sensitive polymeric micelles with different drug distributions: insight from coarse-grained simulations. *ACS Appl. Mater. Interfaces* **2014**, *6*, 17668−17678, DOI: 10.1021/am503920m.
(43) Patel, D.; Bhojani, A. K.; Ray, D.; Singh, D. K.; Bhattacharjee, S.; Seth, D.; Aswal, V. K.; Kuperkar, K.; Bahadur, P. Glucose-induced self-assembly and phase separation in hydrophilic triblock copolymers and the governing mechanism. *Phys. Chem. Chem. Phys.* **2022**, *24*, 21141−21157.
(44) Ji, Y.; Zhu, M.; Gong, Y.; Tang, H.; Li, J.; Cao, Y. Thermoresponsive polymers with lower critical solution temperature-or upper critical solution temperature-type phase behaviour do not induce toxicity to human endothelial cells. *Basic Clin. Pharmacol. Toxicol.* **2017**, *120* (1), 79−85.
(45) Kaizu, K.; Alexandridis, P. Micellization of polyoxyethylene−polyoxypropylene block copolymers in aqueous polyol solutions. *J. Mol. Liq.* **2015**, *210*, 20−28.
(46) Su, Y. L.; Wei, X. F.; Liu, H. Z. Influence of 1-Pentanol on the Micellization of Poly (ethylene oxide)-Poly (propylene oxide)-Poly (ethylene oxide) Block Copolymers in Aqueous Solutions. *Langmuir* **2003**, *19*, 2995−3000.
(47) Hayter, J. B.; Penfold, J. Determination of micelle structure and charge by neutron small-angle scattering. *Colloid Polym. Sci.* **1983**, *261*, 1022−1030.
(48) Ray, D.; Aswal, V. K.; Kohlbrecher, J. Synthesis and characterization of high concentration block copolymer-mediated gold nanoparticles. *Langmuir* **2011**, *27*, 4048−4056.

(49) Joseph, J. P.; Miglani, C.; Bhatt, A.; Ray, D.; Singh, A.; Gupta, D.; Ali, M. E.; Aswal, V. K.; Pal, A. Delineating synchronized control of dynamic covalent and non-covalent interactions for polymer chain collapse towards cargo localization and delivery. *Polym. Chem.* **2021**, *12*, 1002−1013.

(50) Hayter, J. B.; Penfold, J. An analytic structure factor for macroion solutions. *Mol. Phys.* **1981**, *42*, 109−118.

(51) Sikder, A.; Ray, D.; Aswal, V. K.; Ghosh, S. Hydrogen-Bonding-Regulated Supramolecular Nanostructures and Impact on Multivalent Binding. *Angew. Chem.* **2019**, *131*, 1620−1625.

(52) Pedersen, J. S. Analysis of small-angle scattering data from colloids and polymer solutions: modeling and least-squares fitting. *Adv. Colloid Interface Sci.* **1997**, *70*, 171−210.

(53) Bevington, P. R. *Data Reduction and Error Analysis for Physical Sciences*; McGraw-Hill: New York, 1969.

(54) Abraham, M.; Alekseeno, A.; Bergh, C.; Blau, C.; Briland, E.; Doijade, M.; Fleischmann, S.; Gapsys, V.; Garg, G.; Lindahal, E.et al. *GROMACS 2023.3 Source code*; Zenodo, 2023.

(55) Hockney, R. W.; Goel, S. P.; Eastwood, J. W. Quiet high-resolution computer models of a plasma. *J. Comput. Phys.* **1974**, *14* (2), 148−158.

(56) Fontana, C.; Meirelles, J. L.; Verli, H. Indolocarbazoles conformational features and implication in Design of New Bioactive Compounds. *J. Mol. Graphics* **2024**, *124*, 108653−108669, DOI: 10.2139/ssrn.4539332.

(57) Pérez-Sánchez, G.; Schaeffer, N.; Greaves, T. L.; Pereira, J. F.; Coutinho, J. A. Tuning the ionic character of sodium dodecyl sulphate via counter-ion binding: An experimental and computational study. *Front. Mater. Sci.* **2022**, *9*, No. 1011164, DOI: 10.3389/fmats.2022.1011164.

(58) Darden, T.; York, D.; Pedersen, L. Particle mesh Ewald: An N·log (N) method for Ewald sums in large systems. *J. Chem. Phys.* **1993**, *98*, 10089−10092.

(59) Bussi, G.; Donadio, D.; Parrinello, M. Canonical sampling through velocity rescaling. *J. Chem. Phys.* **2007**, *126*, No. 014101, DOI: 10.1063/1.2408420.

(60) Parrinello, M.; Rahman, A. Polymorphic transitions in single crystals: A new molecular dynamics method. *J. Appl. Phys.* **1981**, *52*, 7182−7190.

(61) Martínez, L.; Andrade, R.; Birgin, E. G.; Martínez, J. M. PACKMOL: A package for building initial configurations for molecular dynamics simulations. *J. Comput. Chem.* **2009**, *30*, 2157−2164.

(62) Humphrey, W.; Dalke, A.; Schulten, K. VMD: visual molecular dynamics. *J. Mol. Graph.* **1996**, *14*, 33−38.

(63) Jorge, M. Molecular dynamics simulation of self-assembly of n-Decyltrimethylammonium Bromide micelles. *Langmuir* **2008**, *24*, 5714−5725.

(64) Hoshen, J.; Kopelman, R. Percolation and cluster distribution. I. Cluster multiple labeling technique and critical concentration algorithm. *Phys. Rev. B* **1976**, *14*, 3438−3446.

(65) Elahi, A.; Bidault, X.; Chaudhuri, S. Temperature-transferable coarse-grained model for poly (propylene oxide) to study thermo-responsive behavior of triblock copolymers. *J. Phys. Chem. B* **2016**, *126*, 292−307, DOI: 10.1021/acs.jpcb.1c06318.

(66) Grunewald, F.; Rossi, G.; De Vries, A. H.; Marrink, S. J.; Monticelli, L. Transferable MARTINI model of poly (ethylene oxide). *J. Phys. Chem. B* **2018**, *122* (29), 7436−7449.

(67) Patel, D.; Vaswani, P.; Sengupta, S.; Ray, D.; Bhatia, D.; Choudhury, S. D.; Bahadur, P. Thermoresponsive phase behavior and nanoscale self-assembly generation in normal and reverse Pluronics. *Colloid Polym. Sci.* **2023**, *301*, 75−92, DOI: 10.1007/s00396-022-05039-0.

(68) Tripathi, N.; Singhvi, G.; Roy, A.; Kuperkar, K.; Bahadur, P. Nanoscale Pluronic micellar templates with varying % EO content for controlled drug release and cytotoxicity. *J. Mol. Liq.* **2023**, *384*, 122215−122230.

(69) Vicente, D. S.; Mino, G.; Ramos-Moore, E.; Arancibia-Miranda, N. Effects of Pluronic F68 Micellization on the Viability of Neuronal Cells in Culture. *J. Appl. Polym. Sci.* **2013**, *130*, 2159−2164, DOI: 10.1002/app.39426.

(70) Singla, P.; Singh, O.; Sharma, S.; Betlem, K.; Aswal, V. K.; Peeters, M.; Mahajan, R. K. Temperature-Dependent Solubilization of the Hydrophobic Antiepileptic Drug Lamotrigine in Different Pluronic Micelles-A Spectroscopic, Heat Transfer Method: Small-Angle Neutron Scattering, Dynamic Light Scattering, and in Vitro Release Study. *ACS Omega* **2019**, *4*, 11251−11262.

(71) Zhang, W.; Shi, Y.; Chen, Y.; Ye, J.; Sha, X.; Fang, X. Multifunctional Pluronic P123/F127 mixed polymeric micelles loaded with paclitaxel for the treatment of multidrug resistant tumors. *Biomaterials* **2011**, *32*, 2894−2906.

(72) Parmar, A. V.; Bahadur, A.; Kuperkar, K.; Bahadur, P. PEO-PPO based star-block copolymer T904 as pH responsive nanocarriers for quercetin: Solubilization and release study. *Eur. Polym. J.* **2013**, *49*, 12−21.

(73) Patel, D.; Kuperkar, K.; Yusa, S. I.; Bahadur, P. Nanoscale Self-Assemblies from Amphiphilic Block Copolymers as Proficient Templates in Drug Delivery. *Drugs Drug-Candidates* **2023**, *2*, 898−922.

(74) Li, Z.; Xiong, X.; Peng, S.; Chen, X.; Liu, W.; Liu, C. Novel Floated Pluronic F127 Modified Liposomes for Delivery of Curcumin: Preparation, Release and Cytotoxicity. *J. Microencapsulation* **2019**, *3*, 220−229, DOI: 10.1080/02652048.2020.1720030.

(75) Miki, F.; Kazunori, K.; Keisuke, S.; Yoshiyuki, S.; Hideyuki, S.; Yuichi, T. Enhanced solubility of quercetin by forming composite particles with transglycosylated materials. *J. Food Eng.* **2015**, *149*, 248−254, DOI: 10.1016/j.jfoodeng.2014.10.010.

(76) Riva, A.; Ronchi, M.; Petrangolini, G.; Bosisio, S.; Allegrini, P. Improved Oral Absorption of Quercetin from Quercetin Phytosome: a New Delivery System Based on Food Grade Lecithin. *Eur. J. Drug Metab. Pharmacokinet.* **2019**, *44*, 169−177, DOI: 10.1007/s13318-018-0517-3.

(77) Das, R. K.; Kasoju, N.; Bora, U. Encapsulation of curcumin in alginate-chitosan-pluronic composite nanoparticles for delivery to cancer cells. *Nanomedicine* **2010**, *6*, 153−160.

(78) Wang, Y.; Yu, L.; Han, L.; Sha, X.; Fang, X. Difunctional Pluronic copolymer micelles for paclitaxel delivery: Synergistic effect of folate-mediated targeting and Pluronic-mediated overcoming multidrug resistance in tumor cell lines. *Int. J. Pharm.* **2007**, *337*, 63−73, DOI: 10.1016/j.ijpharm.2006.12.033.

NOTE ADDED AFTER ASAP PUBLICATION

Published ASAP June 7, 2024; Revised June 11, 2024 to correct author name and reorder citations in Methodology.